

Article

Chemical Absorption of CO₂ Enhanced by Nanoparticles Using a Membrane Contactor: Modeling and Simulation

Nayef Ghasem 

Department of Chemical & Petroleum Engineering, UAE University, Al-Ain 15551, UAE; nayef@uaeu.ac.ae

Received: 6 October 2019; Accepted: 8 November 2019; Published: 11 November 2019



Abstract: In the present work, membrane resistance was estimated and analyzed, and the results showed that total membrane resistance increased sharply when membrane pores were wetted. For further study, a two-dimensional (2D) mathematical model was developed to predict the chemical absorption of CO₂ in aqueous methyldiethanolamine (MDEA)-based carbon nanotubes (CNTs) in a hollow fiber membrane (HFM) contactor. The membrane was divided into wet and dry regions, and equations were developed and solved using finite element method in COSMOL. The results revealed that the existence of solid nanoparticles enhanced CO₂ removal rate. The variables with more significant influence were liquid flow rate and concentration of nanoparticles. Furthermore, there was a good match between experimental and modeling results, with the modeling estimates almost coinciding with experimental data. Solvent enhanced by solid nanoparticles significantly improved the separation performance of the membrane contactor. There was around 20% increase in CO₂ removal when 0.5 wt% CNT was added to 5 wt% aqueous MDEA.

Keywords: gas absorption; CO₂ capture; nanofluid; MDEA; membrane wetting; carbon nanotubes (CNTs); global warming

1. Introduction

Gas–liquid hollow fiber membrane (HFM) contactors have attracted the attention of many researchers due to their high interfacial area per unit volume compared to conventional absorption processes. In HFM contactors, mass transfer occurs without dispersion of phases. Shell and tube HFM contactors are employed for the capture of gas impurities, such as CO₂ and H₂S, from natural gas and flue gas. The drawbacks of conventional absorption processes, such as the dispersion of phases, can be avoided in HFM contactors. The disadvantages of packed and tray contactor columns, such as emulsion formation, flooding at high gas flow rates, and weeping at low gas flow rates, can also be avoided in HFM contactors [1–5]. The solvents used in CO₂ absorption and employed by both conventional packed bed columns and membrane contactors are aqueous alkanolamine absorbents. These are the most commonly used absorbents in CO₂ absorption processes, such as CO₂ detention from natural gas, flue gas, and biofuels. Despite the advantages of high absorption performance of alkanolamines, they can cause membrane degradation if used in HFM contactors, corrosion problems if used in industrial gas absorbers, and high-energy consumption during solvent regeneration and circulation. Consequently, researchers have continued to look for better absorbents. Ionic liquid is one of the choices proposed and has been used for CO₂ capture in HFM contactors [6–8]. Another alternative is solid nanoparticles dispersed in water (nanofluids), which also makes for an environmentally friendly substitute absorbent. Distilled water has been found to be enhanced by solid nanoparticles, such as carbon nanotubes (CNTs) and silicon oxide (SiO₂) nanoparticles [9–12]. In [13], the process of using water-based nanoparticles as solvents was modeled considering diffusion in the radial and axial

directions under dry-mode conditions (nonwetting). In [14], CO₂ was found to be absorbed by water that had been enhanced by nanoparticles, such as aluminum oxide, titanium oxide, and silica, in the concentration range of 0.05–0.2 wt%. In the study, the removal of CO₂ from a gas mixture of CO₂/N₂ using nanofluids (metal oxide in distilled water) in a membrane liquid–gas contacting module was examined. Metal oxide nanoparticles, namely, aluminum oxide (Al₂O₃), titanium dioxide (TiO₂), and silicon dioxide (SiO₂), in the concentration range of 0.01–0.2 wt% were experimentally investigated. In [15], a numerical model was established to represent the process of capturing CO₂ from a gas mixture using HMC in distilled water enhanced by carbon nanotubes and nanosilica, mainly at high nanofluid absorbent flow rate. Another study on CO₂ absorption mechanisms for advancements in the use of nanofluids as absorbent in gas–liquid HFM contactors indicated that absorption of CO₂ using nanofluids as absorbent was a challenging method for acid gas removal from gas mixtures [16]. CO₂ absorption from gas mixtures in nanofluids (silica in distilled water) in bubble column absorption has also been investigated [17].

In the area of modeling and simulation of nanofluids, a 2D numerical model was developed for the study of CO₂ gas capture from a gas mixture in a HFM contactor, with water-based nanofluids used as the liquid absorbent [13,18]. The nanofluids that were composed of 0.05 wt% silica nanoparticles were found to enhance separation by around 15%, while a 30% increase was shown using nanofluids composed of distilled water-based CNTs [18]. In [19], a model describing the absorption of CO₂ from a gas mixture in a water-based CNT inside a HFM contactor revealed that absorption of CO₂ was enhanced using solid nanoparticles in water-based solvent. In [20], nanoparticles, such as SiO₂, Al₂O₃, CNT, and Fe₃O₄, were dispersed in distilled water at different concentrations (0.02, 0.05, and 0.1 wt%) and in methyldiethanolamine (MDEA) and diethanolamine (DEA) at concentration of 0.02 wt% to form nanofluids. The prepared nanofluids were used in direct contact with pure CO₂ in a closed vessel at high operating pressures (20, 30, and 40 bar) and a fixed operating temperature of 308 K. In [21], the absorption mechanism of CO₂ in the presence of nanoparticles compared to fresh water were clarified. In [22], holdups of solid nanoparticles, such as CNT, Fe₃O₄, Al₂O₃, and SiO₂, in purified water were used as absorbents for CO₂ in a pilot HFM contactor. In [23], the effect of nanofluids composed of solid nanoparticles on the mass diffusion rate of CO₂ absorption were considered. Experiments and modeling of the process performance of CO₂ capture from gas mixtures using flat sheet membrane contactors were investigated in [24]. In [25], a model of CO₂ removal from natural gas in HFM contactors was developed and solved using COMSOL software package version 5.4 (Comsol AB, Stockholm, Sweden). The model was comprehensive, taking into account momentum, energy, and mass transport, and the model predictions were within the range of the experimental data. An earlier review looked at the absorption of CO₂ in membrane contactors [26]. Absorption of CO₂ from the gas mixture of air/CO₂ in gas–liquid HFM contactors via nanofluids comprising silica nanoparticles and carbon nanotubes were experimental investigated in [27]. Experimental and theoretical studies have also been performed for the absorption of CO₂ in a lab-scale reactor using nanofluids composed of carbon nanotubes. Nanosize Al₂O₃ particles were used, with water and methanol acting as the base fluids [10,28].

In the present work, a comprehensive 2D mathematical model was developed and solved to study the chemical absorption of CO₂ from CO₂/N₂ gas mixture in aqueous MDEA-based CNT inside a HFM contactor, with the model considering partial wetting. As resistance is mainly located in the liquid phase around solid nanoparticles [18], the membrane module was modeled as five subdivisions: two in the tube side (solid-free region and dense phase), two in the membrane (wetted and dry), and one in the shell side (gas phase). The system governing the material balance equations were numerically solved using the finite element method in COMSOL Multiphysics version 5.4. The model predictions were validated with experimental data available in the literature. CO₂ concentration profile was investigated in dry and wetted membrane modes. The effect of operating conditions, such as gas flow rate, liquid flow rate, absorbent size, and concentration, on percentage removal of CO₂ was studied.

2. Mass Transfer Resistance in HFM Contactor

The overall mass transfer resistance ($1/k_G$) in a gas–liquid HFM contactor based on the film theory involves three main resistances in series: liquid phase resistance ($1/k_l$), membrane resistance ($1/k_m$), and resistance of the gas phase boundary layer ($1/k_g$). Accordingly, the overall mass transfer resistance in a HFM contactor is expressed as follows:

$$\frac{1}{k_G} = \frac{d_o}{k_g d_i} + \frac{d_o}{k_m d_{lm}} + \frac{1}{mk_l} \tag{1}$$

where k_g is the mass transfer coefficient in the gas side (m/s); k_m is the mass transfer coefficient in the membrane side (m/s); k_l is the mass transfer coefficient of the liquid phase; d_i , d_o , and d_{lm} are the HFM’s inner, outer, and logarithmic mean diameters, respectively; and m is the dimensionless distribution coefficient at the gas–liquid interface. The mass transfer coefficients k_g and k_l are based on flow conditions and geometry of the HFM contactor [29].

The mass transfer resistance of membrane ($1/k_m$) consists of two resistances: dry membrane resistance ($1/k_{mg}$) and wetted membrane resistance ($1/k_{mw}$), calculated as follows:

$$\frac{1}{k_{mg}} = \frac{\delta \tau}{D_{og} \varepsilon} \tag{2}$$

$$\frac{1}{k_{mw}} = \frac{\delta \tau}{D_{og} \varepsilon} \tag{3}$$

$$\frac{1}{k_m} = \frac{1-y}{k_{mg}} + \frac{y}{k_{mw}} \tag{4}$$

where y is the fraction length of membrane pores filled with solvents; k_{mg} and k_{mw} are the mass transfer coefficient in gas- and liquid-filled pores, respectively; and ε , δ , and τ are the membrane porosity, membrane thickness, and membrane tortuosity, respectively. The liquid mass transfer coefficient is determined using the following relationship:

$$Sh = \sqrt[3]{3.57^3 + 1.62^3 Gz} \tag{5}$$

where Sh is the Sherwood number, and Gz is the Gratz number determined as follows:

$$Sh = k_l d_i / D_l \tag{6}$$

And

$$Gz = \frac{V_l d_i^2}{L D_l} \tag{7}$$

The diffusion coefficient of CO₂ in the liquid phase is determined by the following relationship [30]:

$$D_l (\text{m}^2/\text{s}) = 2.35 \times 10^{-6} \exp\left(-\frac{2119}{T}\right) \tag{8}$$

The diffusion coefficient of CO₂ in the dense liquid film around the nanoparticles is expressed as per Equation (9) [31]:

$$D_n = D_l (1 + 640 Re^{1.7} Sc^{1/3} \phi) \tag{9}$$

where ϕ is the solid volume fraction, and Re is the Reynolds number of the nanosized particles (Brownian motion):

$$Re = \left(\frac{18 k T \rho}{\pi d_p \rho_p \mu^2} \right)^{0.5} \quad (10)$$

where k is the Boltzmann constant (1.38×10^{-23} J/K), T is the temperature in K, ρ is the liquid density, d_p is the particle diameter, ρ_p is the particle density, and μ is the viscosity of the liquid.

The Schmidt number Sc is

$$Sc = \frac{\mu}{\rho D} \quad (11)$$

The mass transfer coefficient in the gas phase, i.e., the gas stream flowing in the shell side, is determined by [32]:

$$Sh_s = 0.34 Re_s^{0.67} Sc_s^{0.33} \quad (12)$$

where Sh_s , Re_s , and Sc_s are the Sherwood number, Reynolds number, and Schmidt number in the shell side, respectively: $Sh_s = k_g d_s / D_g$, $Re_s = \rho_g v_s d_s / \mu_g$, $Sc_s = \mu_g / \rho_g D_g$.

The diffusivity in the gas phase (D_g) is determined using the Chapman–Enskog equation for gas mixture: D_g (m^2/s) = 1.855×10^{-5} . The density of the CO_2/N_2 gas mixture was $343 \text{ kg}/\text{m}^3$, and the viscosity was 1.65×10^{-4} Pa·s. The resistances in series were therefore found to be 5.65×10^4 , 2.67×10^3 , 5.16×10^6 , and $165 \text{ s}/\text{m}$ for the resistances of liquid in the tube side, dry membrane, wetted membrane, and the gas stream in the shell side, respectively. The membrane resistance of the wetted pores was the highest, followed by the liquid phase in the tube side.

3. Mathematical Model

The mathematical model developed in the present work describes the CO_2 concentration profile in a partially wetted HFM contactor, where CO_2 is absorbed in aqueous MDEA-based CNT. The membrane contactor comprises three fragments: tube, membrane, and shell section. The tube side, where the absorbent nanofluid passes through, is divided into two subregions: solid-free zone and dense phase. The gas mixture is transported in the shell side counter-currently with the solvent flow direction (Figure 1a). Figure 1b is the subdivision of the membrane module used to develop the mathematical model equations [28]. CO_2 in the gas phase diffuses through the membrane pores to the nanofluids in the tube side. The ability of N_2 to dissolve in aqueous MDEA solvents is insignificant relative to CO_2 ; subsequently, part of the CO_2 dissolved in the liquid nanofluid is adsorbed on the surface of the solid nanoparticles, and the other portion reacts with MDEA (Figure 1c). The model considers two main mechanisms that generally take place in the presence of nanofluids: the Brownian motion (random motion of particles suspended in a fluid) and the grazing effect [33–35]. The presence of solid nanoparticles in nanofluid enhances the gas absorption due to the adsorption of diffusing gas in the dispersed solid particles. Hence, the gas concentration in the liquid phase near the interface decreases, leading to an increase in the concentration gradient and therefore the absorption rate [16]. Brownian movement increases the velocity near the solid nanoparticle. Microconvection is formed and mass flux dissemination develops, hence altering the diffusion constant [5]. The grazing effect takes place in CO_2 adsorption at the gas–liquid interface in the presence of solid nanoparticles [36].

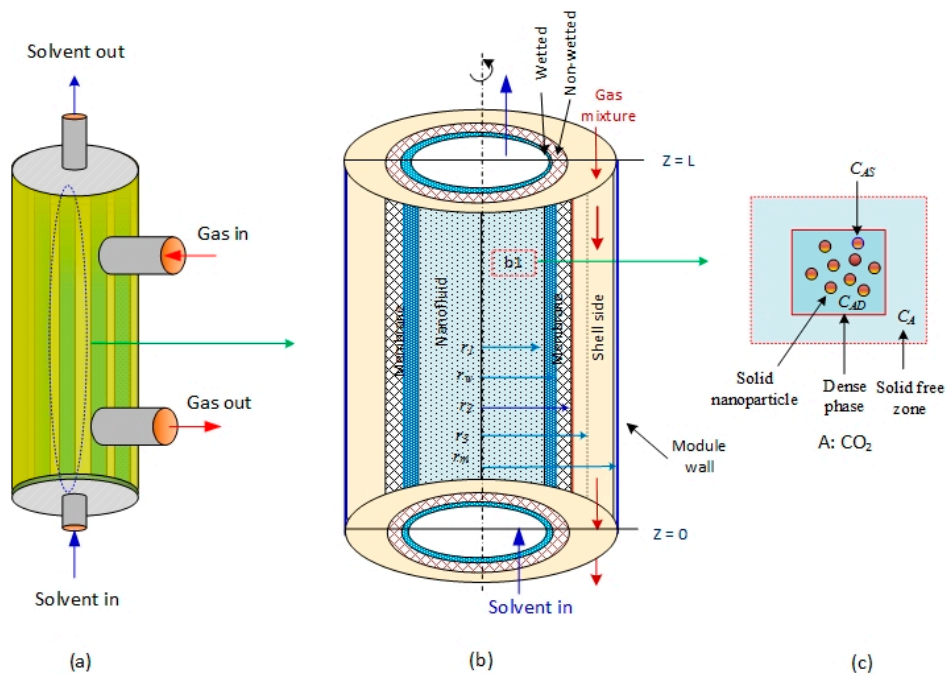


Figure 1. Schematic of the membrane module subdivisions and nanoparticles used in the development of the mathematical model: (a) membrane module, (b) segment used in modeling, and (c) enlargement of box b1 in nanofluid. C_A , C_{AS} , and C_{AD} are the CO_2 concentrations in the solid-free zone, near the solid surface of nanoparticles, and in the dense phase, respectively.

The reaction between acid gases (CO_2) and MDEA has been cited in many articles [3,11,12,37]. There is no hydrogen atom attached to the nitrogen atom in the tertiary amine (MDEA). Hence, CO_2 first dissolves in the water available with the aqueous alkanolamine to form a bicarbonate ion. It can then react with the amine [38]:



The reaction rate of CO_2 is

$$r_{CO_2} = -kC_{CO_2}C_{MDEA} \tag{14}$$

Based on Happel’s free surface [39], laminar gas flow surrounds the membrane tubes. At the Happel’s fictional radius ($r = r_3$), symmetry is considered. The following assumptions were considered in the model development: steady state operation, constant solvent properties, ideal gas, and nanoparticles as homogeneous. The mathematical equations that describe the system behavior were developed for the tube side (solid nanoparticles and liquid), microporous membrane (wetted and dry), and shell side (flow of gas stream). Accordingly, the model equations for the CO_2 diffusion path in the tube, membrane, and shell regions are described in the following subsections.

3.1. Tube Lumen ($0 \leq r \leq r_1$)

The flow of nanofluids (CNT, water, MDEA) in the tube lumen side and the depletion of CO_2 in the lumen side of the membrane take place by absorption of CO_2 in water and by the adsorption of CO_2 on the surface of the nanoparticles and the reaction with aqueous MDEA. Considering the membrane’s partly moisturized section, Equation (15) represents the CO_2 concentration profile in the solid-free zone (C_{CO_2}) with dimensionless radius and length:

$$\frac{D_l}{R^2} \left[\frac{\partial^2 C_{CO_2}}{\partial \varphi^2} + \frac{1}{\varphi} \frac{\partial C_{CO_2}}{\partial \varphi} \right] + \frac{D_l}{L^2} \frac{\partial^2 C_{CO_2}}{\partial \psi^2} - \frac{u_{z1}}{L} \frac{\partial C_{CO_2}}{\partial \psi} = r_{CO_2} \tag{15}$$

The concentration of CO₂ in the dense phase ($C_{CO_2,D}$) is

$$\frac{D_n}{R^2} \left[\frac{\partial^2 C_{CO_2,D}}{\partial \varphi^2} + \frac{1}{\varphi} \frac{\partial C_{CO_2,D}}{\partial \varphi} \right] + \frac{D_n}{L^2} \frac{\partial^2 C_{CO_2,D}}{\partial \psi^2} - \frac{u_{zt}}{L} \frac{\partial C_{CO_2,D}}{\partial \psi} = R_d + r_{CO_2} \quad (16)$$

The dimensionless parameters are symbolized by $\psi = z/L$, $\varphi = r/r_3$.

In Equation (15), D_l is the diffusion coefficient of the CO₂ in the solid-free zone in the tube lumen, D_n is the diffusion coefficient of CO₂ in the dense solid phase, $C_{CO_2,D}$ is the CO₂ concentration in the dense phase, L is the length of the membrane, and R is the radius of the hollow fiber. The adsorption rate, R_d , is as follows:

$$R_d = k_p a_p (C_{CO_2,D} - C_{CO_2,S}) \quad (17)$$

where k_p is the solid–liquid mass transfer coefficient (m/s), a_p is the solid–liquid interfacial area (m²/m³), $C_{CO_2,D}$ is the solute concentration in the suspension (mol/m³), $C_{CO_2,S}$ is the solute concentration at the interface of the particles (mol/m³).

The adsorbed amount of CO₂ on the solid nanoparticles per unit mass of particles, q ($\frac{\text{mol}}{\text{kg}}$), can be given by

$$\phi \rho_p \frac{v_{zt}}{L} \frac{\partial q}{\partial \varphi} = k_p a_p (C_{CO_2,D} - C_{CO_2,S}) \quad (18)$$

where v_{zt} is the velocity in the tube side. The k_p value is estimated from Equation (19). The following correlation is used for mass transfer for flow past single spheres [32]:

$$Sh = 2 + 0.552 Re^{0.5} Sc^{0.33} \quad (19)$$

The value of Sh was found to be 2.08, hence

$$Sh = \frac{k_p d_p}{D_{CO_2}} = 2.08 \quad (20)$$

Then, the k_p value is determined as follows:

$$k_p = 2.08 \times D_{CO_2} / d_p \quad (21)$$

where D_{CO_2} is the CO₂ diffusivity in the solid-free zone. The adsorption of the CO₂ onto the surface of nanoparticles (q) is described by the Langmuir isotherm equation as follows:

$$q = q_m \frac{k_d C_{CO_2,S}}{1 + k_d C_{CO_2,S}} \quad (22)$$

where q ($\frac{\text{mol}}{\text{kg}}$) is the adsorbed amount of CO₂ on solid surface per unit mass of particle, q_m is the highest quantity of adsorbed gas solute, and k_d (m³/mol) is the Langmuir coefficient. The velocity distribution inside the tube (v_{zt}) is assumed to follow Newtonian laminar flow as per Equation (23).

$$v_{zt} = 2v_{zt,avg} \left(1 - \left(\frac{r}{r_1} \right)^2 \right) \quad (23)$$

The appropriate boundary conditions are as follows:

$$\text{inlet of liquid, } z = 0, C_{CO_2} = C_{CO_2,D} = 0 \text{ (fresh solvent)} \quad (24)$$

$$\text{exit of liquid, } z = L, \frac{\partial C_{CO_2}}{\partial \psi} = \frac{\partial C_{CO_2,D}}{\partial \psi} = 0 \text{ (convective flux)} \quad (25)$$

$$\text{tube center, } r = 0, \frac{\partial C_{CO_2}}{\partial \varphi} = \frac{\partial C_{CO_2 D}}{\partial \varphi} = 0 \text{ (axial symmetry)} \tag{26}$$

$$\text{inner radius : } r = r_1, C_{CO_2} = C_{CO_2,wm} \text{ (wetted membrane)} \tag{27}$$

3.2. Membrane ($r_1 \leq r \leq r_2$)

3.2.1. Wetted Membrane Section ($r_1 \leq r \leq r_w$)

The steady-state material balance for the transport of CO₂ is inside the wetted portion of the membrane (there is reaction but no convective term), and diffusion takes place in the wetted membrane. The CO₂ transport in the wetted membrane portion is described by Equation (28):

$$\frac{D_{CO_2,wm}}{R^2} \left[\frac{\partial^2 C_{CO_2,wm}}{\partial \varphi^2} + \frac{1}{\varphi} \frac{\partial C_{CO_2,wm}}{\partial \varphi} \right] + \frac{D_{CO_2,wm}}{L^2} \frac{\partial^2 C_{CO_2,wm}}{\partial \psi} = \epsilon R_{CO_2} \tag{28}$$

where $C_{CO_2,wm}$ is the concentration of CO₂ in the wetted portion of the membrane segment. The diffusivity of CO₂ in the wetted membrane section is determined as follows: $D_{CO_2,wm} = D_l \epsilon / \tau$.

The appropriate boundary conditions in wetted membrane (wm) zone are as follows:

$$\text{tube-wetted membrane interface, } r = r_1, C_{CO_2,wm} = C_{CO_2} \tag{29}$$

$$\text{wetted-dry membrane interface, } r = r_2, C_{CO_2,wm} = m C_{CO_2,m} \tag{30}$$

$$\text{hollow fiber membrane at } z = 0, \frac{\partial C_{CO_2,wm}}{\partial \psi} = 0 \tag{31}$$

$$\text{hollow fiber membrane at } z = L, \frac{\partial C_{CO_2,wm}}{\partial \psi} = 0 \tag{32}$$

3.2.2. Dry Section of the Membrane ($r_w \leq r \leq r_2$)

The CO₂ concentration in the dry part of the membrane, where there is no reaction and no convective term and only diffusion takes place, is calculated as follows:

$$\frac{D_m}{R^2} \left[\frac{\partial^2 C_{CO_2,m}}{\partial \varphi^2} + \frac{1}{\varphi} \frac{\partial C_{CO_2,m}}{\partial \varphi} \right] + \frac{D_m}{L^2} \frac{\partial^2 C_{CO_2,m}}{\partial \psi} = 0 \tag{33}$$

The arbitrary boundary conditions are as follows:

$$\text{wetted-dry membrane interface, } r = r_w, C_{CO_2,m} = C_{CO_2,wm} / m \tag{34}$$

$$\text{membrane-shell interface, } r = r_2, C_{CO_2,m} = C_{CO_2,g} \tag{35}$$

$$\text{membrane bottom edge, } z = 0, \frac{\partial C_{CO_2,m}}{\partial \psi} = 0 \tag{36}$$

$$\text{membrane top edge, } z = L, \frac{\partial C_{CO_2,m}}{\partial \psi} = 0 \tag{37}$$

The diffusivity of CO₂ in the nonwetted membrane section is $D_m = D_g \epsilon / \tau$, where ϵ and τ are the porosity and tortuosity of the membrane, respectively.

3.3. Shell Side ($r_2 \leq r \leq r_3$)

The material balance of the CO₂ in the shell side ($C_{CO_2,g}$), bounded between the membrane's outer skin layer and Happel's free surface model at steady state, is as follows:

$$\frac{D_g}{R^2} \left[\frac{\partial^2 C_{CO_2,g}}{\partial \varphi^2} + \frac{1}{\varphi} \frac{\partial C_{CO_2,g}}{\partial \varphi} \right] + \frac{D_g}{L^2} \frac{\partial^2 C_{CO_2,g}}{\partial \psi^2} - \frac{v_{zs}}{L} \frac{\partial C_{CO_2,g}}{\partial \psi} = 0 \tag{38}$$

The arbitrary boundary conditions are

$$\text{gas inlet side, } z = L, C_{CO_2,g} = C_{CO_2,0} \text{ (inlet CO}_2 \text{ concentration)} \tag{39}$$

$$\text{gas exit side, } z = 0, \frac{\partial C_{CO_2,g}}{\partial \psi} = 0 \text{ (convective flux)} \tag{40}$$

$$\text{free surface, } r = r_3, \frac{\partial C_{CO_2,g}}{\partial \psi} = 0 \text{ (symmetry)} \tag{41}$$

$$\text{shell-membrane interface, } r = r_2 C_{CO_2,g} = C_{CO_2,m} \tag{42}$$

The axial velocity in the shell side is expressed by Happel's free surface model [39]:

$$v_{zs} = 2V_{zs,avg} \left[1 - \left(\frac{r_2}{r_3} \right)^2 \right] \frac{\left(\left(\frac{r}{r_3} \right)^2 - \left(\frac{r_2}{r_3} \right)^2 + 2 \ln \left(\frac{r_2}{r} \right) \right)}{\left(3 + \left(\frac{r_2}{r_3} \right)^4 - 4 \left(\frac{r_2}{r_3} \right)^2 + 4 \ln \left(\frac{r_2}{r_3} \right) \right)} \tag{43}$$

Table 1 lists the parameters used in the numerical solution of the model equations. COSMOL Multiphysics 5.4 was employed to solve the set of partial differential equations.

Table 1. Characteristics of polyvinylidene fluoride (PVDF) membrane module and operating parameters.

Parameter	Value	Reference
Fiber inner radius (m)	2.1×10^{-4}	[40]
Fiber outer radius (m)	5.5×10^{-4}	[40]
Module diameter (m)	0.08	[40]
Module length (m)	0.21	[40]
Total number of fibers	11	[40]
D_l (m ² /s)	$2.35 \times 10^{-6} e^{-\frac{2199}{T}}$	[41]
$D_{CO_2,g}$ (m ² /s)	1.855×10^{-5}	[42]
$D_{CO_2,m}$ (m ² /s)	$D_{CO_2,g} \varepsilon / \tau$	Estimated
$D_{CO_2,wm}$ (m ² /s)	$0.5 D_l$	Estimated
$m = 1/H$	$H = 2.82 \times 10^6 \exp\left(\frac{-2044}{T}\right) / RT$	[41]
Porosity, ε	0.46	[40]
Tortuosity, τ	$(2 - \varepsilon) / \varepsilon$	[24]
k (m ³ /(kmol·s))	$8.741 \times 10^{12} \exp\left(-\frac{8625}{T}\right)$	[43]

The properties of the solid CNT are listed in Table 2.

Table 2. Properties of the solid carbon nanotubes (CNT).

Morphology	Tubular	References
Particle density, ρ_p	2200 kg/m ³	[40]
Particle diameter, d_p	8 nm	[40]
Liquid-solid mass transfer coefficient, k_p	2.6×10^{-3} m/s	[28]
Maximum adsorbed, q_m	29.45 mol/kg	[18]
Specific surface area, a_p	$S_p \times \rho_p$ [1/m]	Estimated
Isotherm constant, Langmuir, k_d	0.49 m ³ /kmol	[18]
CNT weight percent, wt%	0.5%	[40]
Solid surface area, S_p	500 m ² /g	[18]

4. Results and Discussion

Analysis of the mass transfer resistance in the HFM contactor (liquid, membrane, and gas phases) revealed that wetting of membrane pores by the absorbent liquid led to a high increase in the total membrane resistance and hence decreased the percentage removal of CO₂. This can be attributed to the presence of stationary liquid in the wetted piece of the membrane pores, which consequently caused a delay in the CO₂ transport in the membrane holes. Accordingly, the concentration of the CO₂ at the membrane–liquid interface decreased, and the CO₂ removal efficiency also decreased [44]. In the absorbent liquid nanofluid stream in the tube lumen, the liquid–solid mass transfer resistance was low due to the nanosize of the solid nanoparticle; hence, the mass transfer resistance was concentrated in the solid-free liquid region [22].

In order to check the accuracy of the developed mathematical model, the model was validated with our published experimental data obtained for CO₂ absorption from a gas mixture consisting of CO₂/N₂ in aqueous alkanolamine solution with and without solid nanoparticles of carbon nanotubes dispersed in the aqueous MDEA [40]. The model predictions (solid line) for both amine-free aqueous solution (5 wt% MDEA, with the balance being water) and aqueous amine solution with carbon nanotubes (5 wt% MDEA, 0.5 wt% CNT, with the balance being water) are depicted in Figure 2. There was an excellent match between the experimental and simulation results, confirming the promising predictions of the developed model. The deviation of the predicted results from the experimental data was measured using the root mean square error (RMSE) as follows:

$$\text{RMSE} = \left(\frac{\sum E_i^2}{n} \right)^{0.5} \quad (44)$$

where n is the sum of the investigated data points, and E_i^2 is the square of the error between predicted results from the model and experimental data point. The relative error (E_i) was measured as per Equation (45):

$$E_i = \frac{y_{exp} - y_{mod}}{y_{exp}} \quad (45)$$

where y_{exp} and y_{mod} are the experimental and model prediction data points, respectively. The value of the RMSE for the system of aqueous 5 wt% MDEA/water was around 0.01, while it was 0.007 for CNT/MDEA/water. Results revealed that the CO₂ removal rate increased when liquid flow rate increased. This can be attributed to the fact that the thickness of the liquid boundary layer decreased with the increase in liquid flow rate, and the decrease in the liquid boundary layer in the hollow fiber increased the CO₂ diffusion rate into the absorbents. Consequently, the liquid–gas border was kept at low CO₂ concentration (high concentration gradient), which improved the percentage removal of CO₂.

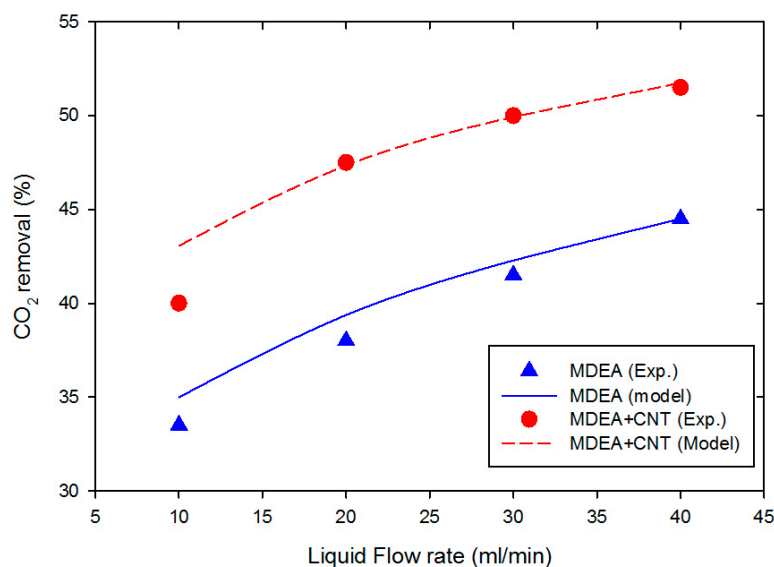


Figure 2. Comparison of developed model predictions (present model) with experimental data [40] for aqueous methyldiethanolamine (MDEA) solution (5 wt%, 0% carbon nanotubes (CNT), with the balance being water) and after adding CNT (5 wt% MDEA, 0.5 wt% CNT, with the balance being water). Gas and liquid flow rates, 10 ml/min; wetting, 0.2%; atmospheric pressure and lab temperature, 25 °C.

At constant liquid flow rate, the effect of flow rate of gas (GFR) on the percentage removal of CO₂ is depicted in Figure 3. It can be seen that the percentage removal at a fixed liquid flow rate was not evenly spaced; rather, as expected, the percentage removal of carbon dioxide decreased at high gas flow rates. With the increase in gas volumetric flow rate from 10 to 20 mL/min, a sharp decrease in percentage removal of CO₂ from 45 to 25% occurred. This can be attributed to the decrease in the residence time of the gas stream in the shell side of the hollow fiber membrane, which negatively influenced the effectiveness of CO₂ separation in the membrane contactor. The percentage removal of CO₂ (η) can be obtained as per Equation (46):

$$\eta = \frac{C_{in}Q_{in} - C_{out}Q_{out}}{C_{in}Q_{in}} \times 100 \tag{46}$$

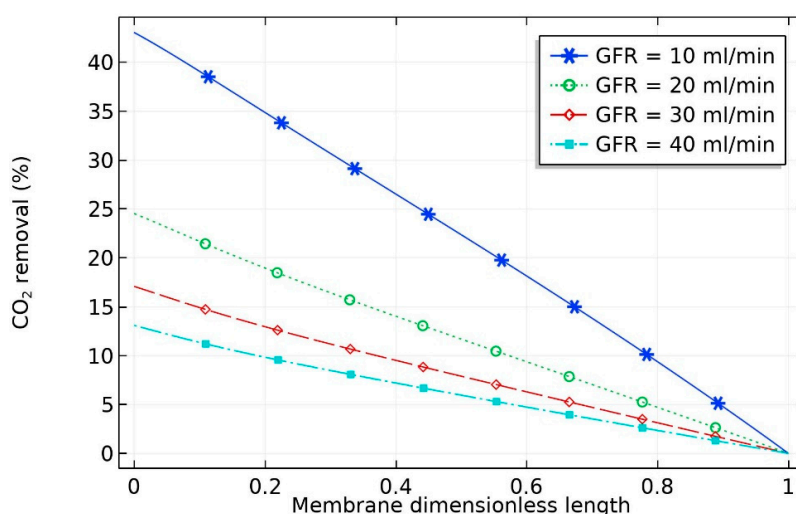


Figure 3. Effect of inlet gas volumetric flow rate (GFR) on the percentage removal of CO₂ at a fixed liquid flow rate (10 mL/min) and solvent composition (0.5 wt% CNT, 5 wt% MDEA, and 20 vol% CO₂).

The influence of feed flow rate of gas on CO₂ removal flux is shown in Figure 4. Increasing gas velocity improved the gas mass transfer coefficient and hence increased the CO₂ withdrawal flux [24]. This can be attributed to the fact that the gas mass transfer coefficient is directly related to the gas velocity [18]. The CO₂ removal flux, which is used to indicate the process efficiency, can be estimated by the following equation:

$$J_{CO_2} \left(\frac{\text{mol}}{\text{m}^2 \cdot \text{s}} \right) = \frac{(y_{CO_2,in} Q_{in} - y_{CO_2,out} Q_{out}) \times 273.15 \times 1000}{22.4 \times T_g \times A_T} \tag{47}$$

where J_{CO_2} is the CO₂ removal flux; $y_{CO_2,in}$ and $y_{CO_2,out}$ are the inlet and exit CO₂ mole fraction, respectively; Q_{in} and Q_{out} (m³/s) represent the inlet and exit volumetric flow rate of gas in the gas phase, respectively; T_g (K) is the real gas temperature; and A_T (m²) represents the membrane area at the liquid–gas interface.

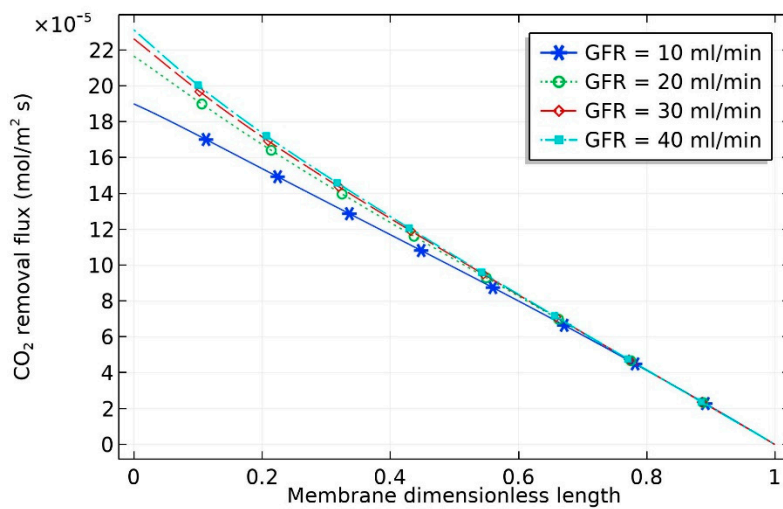


Figure 4. Effect of inlet GFR on the percentage removal of CO₂ in the hollow fiber membrane (HFM) contactor system (0.5 wt% CNT, 5 wt% MDEA, 20 vol% CO₂).

As can be seen from the figure, there was a significant increase in CO₂ removal flux when the liquid flow rate increased from 10 to 20 mol/min, with the removal flux increasing from 1.9×10^{-4} to 2.2×10^{-4} mol/m²·s. By contrast, the increase in molar flux was insignificant when the liquid flow rate increased from 20 to 40 mL/min. This can be attributed to the drop in the CO₂ concentration gradient with increasing liquid flow rate. The crosswise contour of CO₂ concentration in the HFM contactor is predicted in Figure 5. The inlet liquid and gas flow rates were both fixed at 10 ml/min. The feed stream contained 20 vol% CO₂ in the CO₂/N₂ gas mixture. The inlet nanofluid contained dispersed CNT in aqueous MDEA solution (5 wt% MDEA, 0.5 wt% CNT, with the balance being water). The diagram reveals that there was a drop in the CO₂ volume in the inlet gas stream. It dropped downward in the shell side of the membrane from 20 to around 5 vol%.

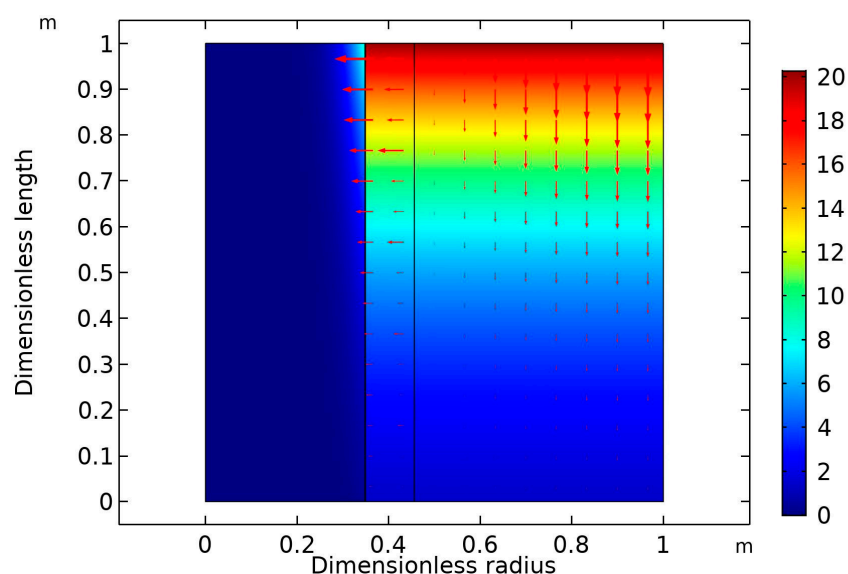


Figure 5. Surface plot diagram of the CO₂ volume percentage through the HMC at equal inlet gas and liquid flow rates (10 mL/min), nanofluid composition (0.5 wt% CNT, 5 wt% MDEA, with the balance being water), and feed gas composition (20 vol% CO₂). Arrows represent convective flux.

Figure 6 is the surface plot of the CO₂ volume at high gas flow rate (30 mL/min) and fixed liquid flow rate (10 mL/min). As expected, the higher the gas velocity, the lower was the CO₂ removal rate [36]. In this case, the percentage removal of CO₂ dropped from 90% (GFR = 10 mL/min) to around 60% (GFR = 30 mol/min).

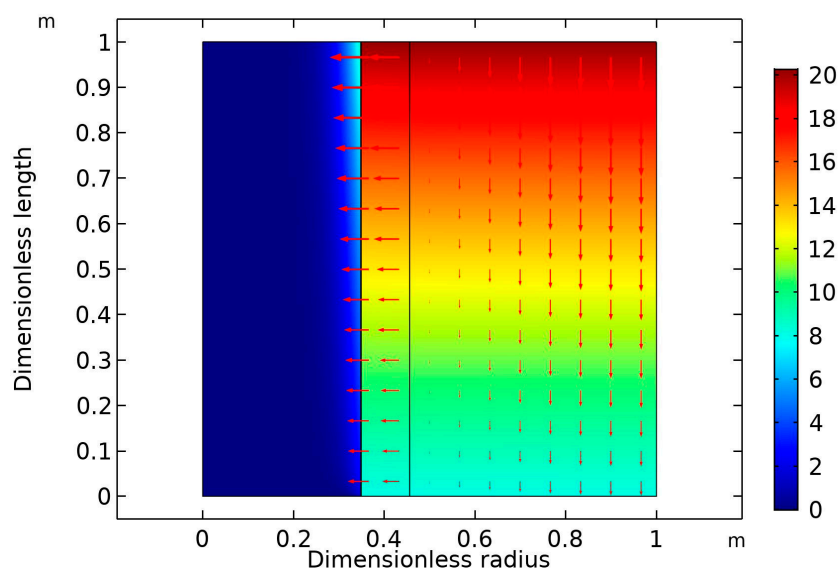


Figure 6. Surface plot of the CO₂ volume percentage through the membrane separation process at constant gas and liquid flow rates (30 and 10 mL/min, respectively), nanofluid composition (0.5 wt% CNT), and liquid and gas feed composition (5 wt% MDEA, 20 vol% CO₂). Arrows represent convective flux.

Figure 7 displays the effect of membrane wetting on the percentage removal of CO₂ at variable gas volumetric flow rates and fixed liquid flow rate (10 mL/min). The diagram reveals that the percentage wetting of membrane had a significant impact on the percentage removal of CO₂. As the wetted membrane portion increased, the percentage removal of CO₂ decreased. This can be attributed to the fact that the membrane resistance increased with membrane wetting because the diffusion coefficient

of gas in the wetted membrane (liquid-filled pores) was much lower than the CO₂ diffusion in the dry membrane (gas-filled pores). At fixed membrane wetting, as the gas flow rate increased, the percentage removal of CO₂ decreased. This can be attributed to the fact that, as the gas flow rate increased, the gas residence time in the membrane shell side decreased, thereby reducing the chance of gas molecules to come into direct contact with liquid at the gas-liquid interface.

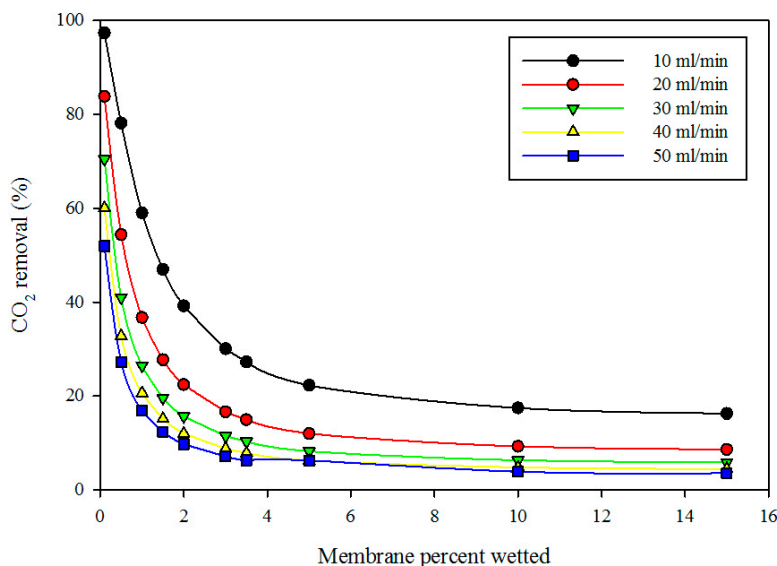


Figure 7. Model predictions of the effect of wetted membrane percentage on the percentage removal of CO₂ at variable gas flow rate and fixed liquid flow rate (10 mL/min).

The effect of nanoparticle volume fraction on the solvent is depicted in Figure 8. The diagram reveals that the percentage removal of CO₂ increased with solid nanoparticles, which can be attributed to the grazing effect (increase in the amount of CO₂ adsorbed into the surface of the CNT). The increase would be limited by obtaining a homogeneous solvent, but this is not achievable for high CNT concentration [36].

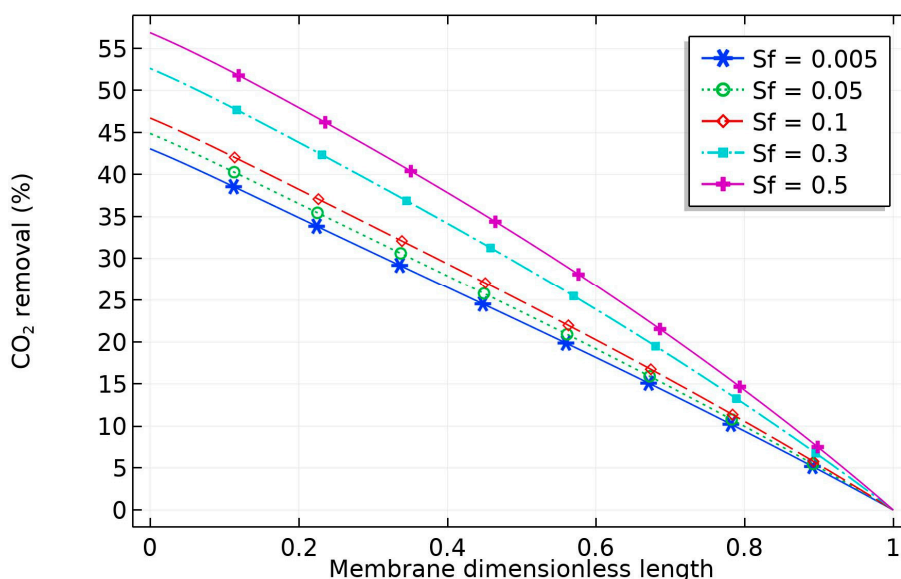


Figure 8. Effect of CNT volume fraction on the percentage removal of CO₂. Liquid and gas flow rates were both 10 mL/min. The solvent contained variable volume fraction of CNT, 5 wt% MDEA, with the balance being water. The feed gas contained 20 vol% CO₂, with the balance being N₂.

5. Conclusions

The present work aimed to study the chemical absorption process of CO₂ from CO₂/N₂ gas mixture in aqueous MDEA-based CNT in a HFM contactor. The membrane resistance was studied, and the results showed that wetted membrane pores significantly increased the membrane resistance. A steady-state 2D mathematical model was developed considering partially wetted membrane. The effect of gas flow rate, liquid flow rate, nanoparticle volume fraction, and membrane wetting on CO₂ removal rate and CO₂ removal flux was investigated. The tube side was modeled as a solid-free zone and a dense phase, while the shell side was modeled as a single gas phase. The model governing the equations were solved using finite element method built in COSMOL Multiphysics version 5.4. The predicted results revealed that the existence of solid nanoparticles enhanced the CO₂ removal rate. The present model offered a good basis to explore the performance of CO₂ capture in the presence of nanoparticles in reactive solvent (MDEA). The CO₂ removal rate increased with solid concentration. The simulation results revealed that liquid flow rate and concentration of nanoparticles had a strong impact on the CO₂ absorption and hence the CO₂ removal efficiency and removal flux. The model predictions and the experimental data were compared and found to be in good agreement.

Funding: This research was funded by United Arab Emirates University, UAE, UPAR grant number 31N374.

Acknowledgments: The author acknowledged the financial support provided by UAEU.

Conflicts of Interest: The authors declare no conflict of interest.

References

1. Gabelman, A.; Hwang, S.T. Hollow fiber membrane contactors. *J. Membr. Sci.* **1999**, *159*, 61–106. [[CrossRef](#)]
2. Iversen, S.B.; Bhatia, V.K.; Dam-Johansen, K.; Jonsson, G. Characterization of microporous membranes for use in membrane contactors. *J. Membr. Sci.* **1997**, *130*, 205–217. [[CrossRef](#)]
3. Yan, S.P.; Fang, M.X.; Zhang, W.F.; Wang, S.Y.; Xu, Z.K.; Luo, Z.Y.; Cen, K.F. Experimental study on the separation of CO₂ from flue gas using hollow fiber membrane contactors without wetting. *Fuel Process. Technol.* **2007**, *88*, 501–511. [[CrossRef](#)]
4. Keshavarz, P.; Fathikalajahi, J.; Ayatollahi, S. Analysis of CO₂ separation and simulation of a partially wetted hollow fiber membrane contactor. *J. Hazard. Mater.* **2008**, *152*, 1237–1247. [[CrossRef](#)] [[PubMed](#)]
5. Xuan, Y. Conception for enhanced mass transport in binary nanofluids. *Heat Mass Transf. Waerme Und Stoffuebertragung* **2009**, *46*, 277–279. [[CrossRef](#)]
6. Qazi, S.; Gómez-Coma, L.; Albo, J.; Druon-Bocquet, S.; Irabien, A.; Sanchez-Marcano, J. CO₂ capture in a hollow fiber membrane contactor coupled with ionic liquid: Influence of membrane wetting and process parameters. *Sep. Purif. Technol.* **2020**, *233*, 115986. [[CrossRef](#)]
7. Albo, J.; Luis, P.; Irabien, A. Carbon dioxide capture from flue gases using a cross-flow membrane contactor and the ionic liquid 1-ethyl-3-methylimidazolium ethylsulfate. *Ind. Eng. Chem. Res.* **2010**, *49*, 11045–11051. [[CrossRef](#)]
8. Taylor, P.; Albo, J.; Luis, P.; Irabien, A. Absorption of coal combustion flue gases in ionic liquids using different membrane contactors. *Desalin. Water Treat.* **2011**, *27*, 54–59.
9. Alper, E.; Wichtendahl, B.; Deckwer, W.-D. Gas absorption mechanism in catalytic slurry reactors. *Chem. Eng. Sci.* **1980**, *35*, 217–222. [[CrossRef](#)]
10. Torres Pineda, I.; Lee, J.W.; Jung, I.; Kang, Y.T. CO₂ absorption enhancement by methanol-based Al₂O₃ and SiO₂ nanofluids in a tray column absorber. *Int. J. Refrig.* **2012**, *35*, 1402–1409. [[CrossRef](#)]
11. Hedayat, M.; Soltanieh, M.; Mousavi, S.A. Simultaneous separation of H₂S and CO₂ from natural gas by hollow fiber membrane contactor using mixture of alkanolamines. *J. Membr. Sci.* **2011**, *377*, 191–197. [[CrossRef](#)]
12. Sohrabi, M.R.; Marjani, A.; Moradi, S.; Davallo, M.; Shirazian, S. Mathematical modeling and numerical simulation of CO₂ transport through hollow-fiber membranes. *Appl. Math. Model.* **2011**, *35*, 174–188. [[CrossRef](#)]

13. Rezakazemi, M.; Darabi, M.; Soroush, E.; Mesbah, M.; Dai, Z.; Usman, M.; Hillestad, M.; Deng, L.; Ghasem, N.; Al-Marzouqi, M.; et al. CO₂ absorption enhancement by water-based nanofluids of CNT and SiO₂ using hollow-fiber membrane contactor. *Sep. Purif. Technol.* **2019**, *210*, 920–926. [[CrossRef](#)]
14. Mohammaddoost, H.; Azari, A.; Ansarpour, M.; Osfouri, S. Experimental investigation of CO₂ removal from N₂ by metal oxide nanofluids in a hollow fiber membrane contactor. *Int. J. Greenh. Gas. Control.* **2018**, *69*, 60–71. [[CrossRef](#)]
15. Hajilary, N.; Rezakazemi, M. CFD modeling of CO₂ capture by water-based nanofluids using hollow fiber membrane contactor. *Int. J. Greenh. Gas. Control.* **2018**, *77*, 88–95. [[CrossRef](#)]
16. Zhang, Z.; Cai, J.; Chen, F.; Li, H.; Zhang, W.; Qi, W. Progress in enhancement of CO₂ absorption by nanofluids: A mini review of mechanisms and current status. *Renew. Energy* **2018**, *118*, 527–535. [[CrossRef](#)]
17. Darvanjooghi, M.H.K.; Esfahany, M.N.; Esmaili-Faraj, S.H. Investigation of the effects of nanoparticle size on CO₂ absorption by silica-water nanofluid. *Sep. Purif. Technol.* **2018**, *195*, 208–215. [[CrossRef](#)]
18. Darabi, M.; Rahimi, M.; Molaei Dehkordi, A. Gas absorption enhancement in hollow fiber membrane contactors using nanofluids: Modeling and simulation. *Chem. Eng. Process. Process. Intensif.* **2017**, *119*, 7–15. [[CrossRef](#)]
19. Koronaki, I.P.; Nitsas, M.T.; Vallianos, C.A. Enhancement of carbon dioxide absorption using carbon nanotubes—A numerical approach. *Appl. Therm. Eng.* **2016**, *99*, 1246–1253. [[CrossRef](#)]
20. Rahmatmand, B.; Keshavarz, P.; Ayatollahi, S. Study of Absorption Enhancement of CO₂ by SiO₂, Al₂O₃, CNT, and Fe₃O₄ Nanoparticles in Water and Amine Solutions. *J. Chem. Eng. Data* **2016**, *61*, 1378–1387. [[CrossRef](#)]
21. Haghtalab, A.; Mohammadi, M.; Fakhroueian, Z. Absorption and solubility measurement of CO₂ in water-based ZnO and SiO₂ nanofluids. *Fluid Phase Equilibria* **2015**, *392*, 33–42. [[CrossRef](#)]
22. Peyravi, A.; Keshavarz, P.; Mowla, D. Experimental Investigation on the Absorption Enhancement of CO₂ by Various Nanofluids in Hollow Fiber Membrane Contactors. *Energy Fuels* **2015**, *29*, 8135–8142. [[CrossRef](#)]
23. Kim, J.H.; Jung, C.W.; Kang, Y.T. Mass transfer enhancement during CO₂ absorption process in methanol/Al₂O₃ nanofluids. *Int. J. Heat Mass Transf.* **2014**, *76*, 484–491. [[CrossRef](#)]
24. Ghasem, N.; Al-Marzouqi, M. Modeling and experimental study of carbon dioxide absorption in a flat sheet membrane contactor. *J. Membr. Sci. Res.* **2017**, *3*, 57–63.
25. Ghasem, N.; Al-Marzouqi, M.; Abdul Rahim, N. Modeling of CO₂ absorption in a membrane contactor considering solvent evaporation. *Sep. Purif. Technol.* **2013**, *110*, 1–10. [[CrossRef](#)]
26. Zhang, Z.E.; Yan, Y.F.; Zhang, L.; Ju, S.X.; Yan, Y.F.; Zhang, L.; Ju, S.X. Hollow Fiber Membrane Contactor Absorption of CO₂ From the Flue Gas: Review and Perspective. *Glob. Nest J.* **2014**, *16*, 354–373.
27. Golkhar, A.; Keshavarz, P.; Mowla, D. Investigation of CO₂ removal by silica and CNT nanofluids in microporous hollow fiber membrane contactors. *J. Membr. Sci.* **2013**, *433*, 17–24. [[CrossRef](#)]
28. Lu, S.; Xing, M.; Sun, Y.; Dong, X. Experimental and Theoretical Studies of CO₂ Absorption Enhancement by Nano-Al₂O₃ and Carbon Nanotube Particles. *Chin. J. Chem. Eng.* **2013**, *21*, 983–990. [[CrossRef](#)]
29. Mosadegh-Sedghi, S.; Félix, S.; Mendes, A. Determination of CO₂ Absorption Kinetics in Amino Acid Salts Solutions Using Membrane Contactors. *Int. J. Membr. Sci. Technol.* **2017**, *4*, 8–18.
30. Versteeg, G.F.; van Swaaij, W.P.M. On the kinetics between CO₂ and alkanolamines both in aqueous and non-aqueous solutions-II. Tertiary amines. *Chem. Eng. Sci.* **1988**, *43*, 587–591. [[CrossRef](#)]
31. Villeneuve, K.; Albarracin Zaidiza, D.; Roizard, D.; Rode, S.; Nagy, E.; Feczko, T.; Koroknai, B. Enhancement of oxygen mass transfer rate in the presence of nanosized particles. *Chem. Eng. Sci.* **2007**, *62*, 7391–7398.
32. Geankoplis, C.J. *Transport. Processes and Separation Process Principle*, 4th ed.; Prentice Hall: Upper Saddle River, NJ, USA, 2003; ISBN 978-0131013674.
33. Kars, R.L.; Best, R.J.; Drinkenburg, A.A.H. The sorption of propane in slurries of active carbon in water. *Chem. Eng. J.* **1979**, *17*, 201–210. [[CrossRef](#)]
34. Kluytmans, J.H.J.; van Wachem, B.G.M.; Kuster, B.F.M.; Schouten, J.C. Mass transfer in sparged and stirred reactors: Influence of carbon particles and electrolyte. *Chem. Eng. Sci.* **2003**, *58*, 4719–4728. [[CrossRef](#)]
35. Brillman, D.W.F.; Van Swaaij, W.P.M.; Versteeg, G.F. A one-dimensional instationary heterogeneous mass transfer model for gas absorption in multiphase systems. *Chem. Eng. Process. Process. Intensif.* **1998**, *37*, 471–488. [[CrossRef](#)]
36. Ghasem, N. Modeling and Simulation of CO₂ Absorption Enhancement in Hollow-Fiber Membrane Contactors using CNT–Water–Based Nanofluids. *J. Membr. Sci. Res.* **2019**, *5*, 295–302.

37. Fu, D.; Zhang, P.; Mi, C. Effects of concentration and viscosity on the absorption of CO₂ in [N1111][Gly] promoted MDEA (methyldiethanolamine) aqueous solution. *Energy* **2016**, *101*, 288–295. [[CrossRef](#)]
38. Ko, J.J.; Li, M.H. Kinetics of absorption of carbon dioxide into solutions of N-methyldiethanolamine + water. *Chem. Eng. Sci.* **2000**, *55*, 4139–4147. [[CrossRef](#)]
39. Happel, J. Viscous flow relative to arrays of cylinders. *Aiche J.* **1959**, *5*, 174–177. [[CrossRef](#)]
40. Rehman, Z.U.; Ghasem, N.; Al-Marzouqi, M.; Abdullatif, N. Enhancement of Carbon Dioxide Absorption using Nanofluids in Hollow Fiber Membrane Contactor. *Chin. J. Chem. Eng.* **2019**, in press. [[CrossRef](#)]
41. Versteeg, G.F.; van Swaal, W.P.M. Solubility and Diffusivity of Acid Gases (CO₂, N₂O) in Aqueous Alkanolamine Solutions. *J. Chem. Eng. Data* **1988**, *33*, 29–34. [[CrossRef](#)]
42. Cussler, E.L. *Diffusion Mass Transfer in Fluid Systems*, 3rd ed.; Cambridge University: New York, NY, USA, 2009; ISBN 9780521871211.
43. Wang, R.; Li, D.F.; Liang, D.T. Modeling of CO₂ capture by three typical amine solutions in hollow fiber membrane contactors. *Chem. Eng. Process. Process. Intensif.* **2004**, *43*, 849–856. [[CrossRef](#)]
44. Zhang, H.-Y.; Wang, R.; Liang, D.T.; Tay, J.H. Theoretical and experimental studies of membrane wetting in the membrane gas–liquid contacting process for CO₂ absorption. *J. Membr. Sci.* **2008**, *308*, 162–170. [[CrossRef](#)]



© 2019 by the author. Licensee MDPI, Basel, Switzerland. This article is an open access article distributed under the terms and conditions of the Creative Commons Attribution (CC BY) license (<http://creativecommons.org/licenses/by/4.0/>).